Analytical theory and control of the longitudinal dynamics of a storage-ring free-electron laser

Giovanni De Ninno[1] and Duccio Fanelli[2]
[1]*Sincrotrone Trieste, 34012 Trieste, Italy*
[2]*Cell and Molecular Biology Department, Karolinska Institute, SE-171 77 Stockholm, Sweden*
(Received 31 January 2004; published 9 July 2004)

A comprehensive analytical description is given of the longitudinal dynamics of a storage-ring free-electron laser in the presence of a finite light-electron beam temporal detuning. Closed analytical expressions for the main statistical parameters of the system (i.e., beam energy spread, intensity, centroid position, and r.m.s. value of the laser distribution) as a function of the detuning are provided. The transition between the stable "cw" regime and the unstable steady state is shown to be a Hopf bifurcation. This allows us to introduce a feedback procedure which suppresses the bifurcation and significantly improves the system stability. The critical value of the detuning above which the bifurcation occurs is analytically derived as a function of the electron energy and of the beam optics parameters. Results are compared to experiments and display good agreement. Comparisons with other theoretical models are also drawn.

DOI: 10.1103/PhysRevE.70.016503 PACS number(s): 41.60.Cr, 29.20.Dh, 05.45.−a

I. INTRODUCTION

A free-electron laser (FEL) is very closely related to the undulator insertion devices familiar to all third generation light source users. A relativistic electron beam interacts with an electromagnetic field as it passes through a periodic magnetic structure forcing particles to move along sin-like trajectories and, consequently, to emit radiation. Depending on their initial phases, electrons gain or lose energy after the interaction and this leads to a clustering further downstream. This microbunching is, in turn, the source of enhanced (coherent) radiation emission. The term FEL actually covers a wide variety of configurations. FEL oscillators (implemented both on storage rings and on LINACs) have been the first ones to be operated [1,2] and are still by far the common ones. They provide intense, tunable, monochromatic, and fully coherent radiation in the range from the infrared to the UV/VUV. The quality of the optical cavity mirrors is presently the limiting factor for the performance of such devices. In particular, it appears clear that the ambitious goal of obtaining laser light in the x-ray region rests on the successful evolution of other kinds of FELs not employing mirrors, such as self-amplified spontaneous emission (SASE) (see Ref. [3] for a complete list of references) or high gain harmonic generation (HGHG) [4]. Nevertheless, in the spectral regions where high reflectivity mirrors are available, FEL oscillators represent excellent light sources for scientific research [5,6] because they can reach a spectral purity and a temporal stability which at present does not seem to be achievable with other techniques. Among oscillators, storage-ring FELs (SRFELs, whose layout is schematically shown in Fig. 1, present by far the more complex dynamics. Such complexity origins from the fact that, unlike LINAC-based FELs, where the electron beam is renewed after each passage inside the interaction region, electrons are recirculated.

As a result, at every light-beam energy exchange the system keeps memory of previous interactions. In a SRFEL the light produced by the electron beam is stored in an optical cavity and amplified during the successive turns of the particles in the ring. The electron-beam energy is maintained constant by means of a device (the radio frequency) which supplies, turn by turn, the energy lost due to synchrotron and FEL radiation to the electrons. The amplification is obtained to the detriment of the electron-beam energy spread which becomes larger when the intracavity power grows. The heating of the electron bunch due to the laser onset leads to the reduction of the amplification gain until the latter reaches the level of the cavity losses (laser saturation).

Since it originates from the synchrotron radiation, the laser is naturally pulsed at the electron beam revolution period (hundred of ns). On a larger (millisecond) temporal scale the FEL dynamics depends strongly on the longitudinal overlap between the electron bunch(es) and the laser pulses at each pass inside the optical cavity. A given temporal detuning, i.e., a difference between the electron beam revolution period and the photons round trip inside the optical cavity, leads to a cumulative delay between the electrons and the laser pulses: the laser intensity may then appear "cw" (for a weak or strong detuning) or show a pulsed behavior (for an intermediate detuning amount) [7,8]. The temporal detuning can be experimentally controlled either modifying the electron-beam revolution period (via the variation of the radio frequency) or by changing the distance between the mirrors of the optical cavity. Due to a better sensitivity, the former method is generally preferred. The central, narrow, "cw" zone of the detuning curve (few fs around the perfect synchronism) is generally the most interesting for user applications: in this zone, the laser is indeed characterized by the maximum average power and the signal is the closest to the Fourier limit [9]. However, it is worth mentioning that the "ideal" dynamics, namely, the existence of a stable regime around the perfect tuning, is a peculiar characteristic of second-generation SRFELs, such as Super-ACO and UVSOR. Last-generation SRFELs, such as DUKE and ELETTRA, do not seem, at present, to display a similar behavior [10,11]. In fact, the existence of a reproducible, stable, regime has not yet been experimentally observed. The reason for that can be mainly traced back to the increased sensitivity to electron-beam instabilities, which is proper to

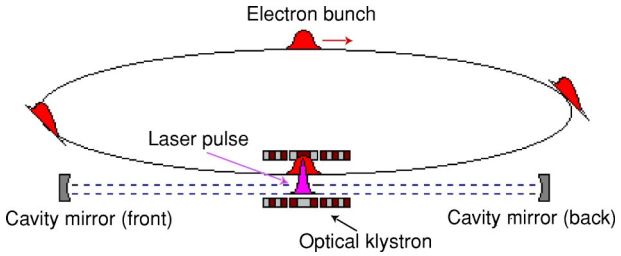

FIG. 1. Schematic layout of a SRFEL.

"high-gain" SRFELs with respect to lower-gain devices of previous generation. In order to keep the laser-electron beam synchronism and avoid jittering, which could determine a migration towards one of the unstable, pulsed zones of the detuning curve, the Super-ACO and UVSOR SRFELs have implemented dedicated feedback systems [12,13]. These kind of devices assume the existence of a stable "cw" regime and, for this reason, cannot be straightforwardly installed on last-generation SRFELs.

The longitudinal dynamics of a SRFEL in the central "cw" zone of the detuning curve has been discussed in a number of papers. The most significant analytical results have been obtained in Refs. [14,15]. Here the laser electric field, assumed to be centered around the maximum of the temporal electron-bunch distribution, is decomposed on a basis of longitudinal modes (the so-called "super modes") self-reproducing in form after each round trip. After many beam revolutions, the system spontaneously evolves towards the fundamental super mode, which is characterized by a Gaussian profile. In most cases, this result has been found to be in a good agreement with experiments [16,17].

Up to now, due to the high mathematical complexity of the problem, the longitudinal FEL dynamics in presence of a significant laser-electron beam detuning has been studied only numerically. Two different kinds of models have been developed. In the first, the single-particle motion inside the electron bunch and the dynamics of the field amplitude and phase have been explicitly taken into account [18–20]. The others, consider only the evolution of the statistical parameters of the electron bunch (i.e., the bunch length and the energy spread) and of the laser distribution (i.e., intensity, centroid position, and r.m.s. value) [21–24].

The model presented in Ref. [21,23] belongs to the second category and is the starting point of this study. This paper represents a natural complement to Ref. [25] and it is organized as follows. In Sec. II the starting model is briefly reviewed. In Sec. III an explicit four-dimensional discrete map is introduced, based on the assumption of a Gaussian profile for the laser distribution. In Sec. IV, the formulation is further simplified: by means of a Taylor development four rate equations are obtained and shown to be particularly suitable for an analytical investigation. Section V is devoted to the study of the fixed points of the system as a function of the detuning parameter. Closed analytical expressions are provided and compared to results from numerical simulations. In Sec. VI, these theoretical predictions are compared, for the case of the perfect tuning, to experiments carried out on the Super-ACO and ELETTRA FELs and with the estimate obtained in the framework of the super-mode

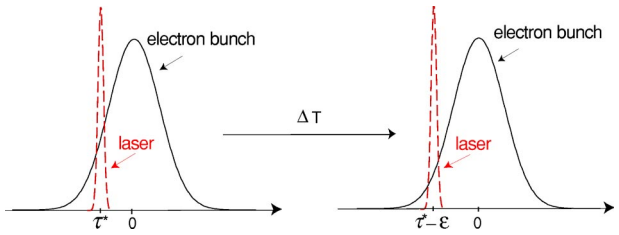

FIG. 2. Schematic layout of the pass-to-pass laser-electron beam interaction. ΔT stands for the period between two successive interactions, τ^* is the position of the laser centroid with respect to the peak of the electron density, and ϵ accounts for the laser-electron beam detuning at each pass.

theory. In Sec. VII the study of the stability of the fixed points is performed. The transition between the "cw" and the pulsed regimes is shown to be a Hopf bifurcation. This result is exploited in Sec. VIII where a feedback procedure is introduced and shown to enlarge the FEL stability domain. Finally, in Sec. IX an explicit analytical expression of the critical detuning is derived and compared with experiments and with the super-mode theory predictions. In order to relieve the main text, the details of the calculations are reported in the Appendixes.

II. THE ORIGINAL MODEL

The longitudinal dynamics of a SRFEL can be described by a system of rate equations accounting for the coupled evolution of the electromagnetic field and of the longitudinal parameters of the electron bunch [21]. The temporal profile of the laser intensity y_n is updated at each pass n inside the optical cavity according to

$$y_{n+1}(\tau) = R^2 y_n(\tau - \epsilon)[1 + g_n(\tau)] + i_s(\tau), \tag{1}$$

where τ is the temporal position of the electron bunch distribution with respect to the centroid, R is the mirror reflectivity, the detuning parameter ϵ is the difference between the electrons revolution period (divided by the number of bunches) and the period of the photons inside the cavity, $i_s(\tau)$

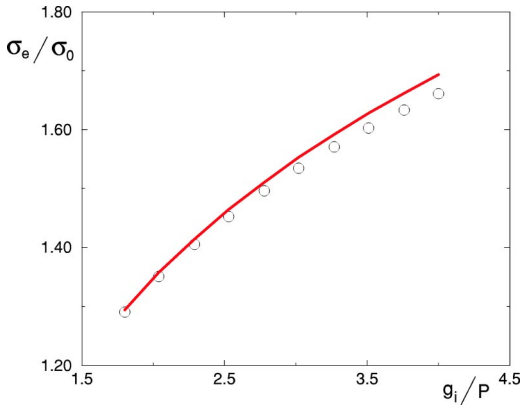

FIG. 3. σ_e/σ_0 is plotted versus the ratio g_i/P. The circles represent the numerical solution of Eq. (5) while the solid line refers to the theoretical estimate (9). The difference keeps smaller than 2%.

accounts for the profile of the spontaneous emission of the optical klystron [26,27]. Figure 2 shows a schematic layout of the light-electron beam interaction in the presence of a finite detuning ϵ.

The FEL gain $g_n(\tau)$ is given by

$$g_n(\tau) = g_i \frac{\sigma_0}{\sigma_n} \exp\left[- \frac{\sigma_n^2 - \sigma_0^2}{2\sigma_0^2} \right] \exp\left[- \frac{\tau^2}{2\sigma_{\tau,n}^2} \right], \qquad (2)$$

where g_i and σ_0 are the initial (laser-off) peak gain and beam energy spread, while σ_n and $\sigma_{\tau,n}$ are the energy spread and the bunch length after the nth light-electron beam interaction. The first exponential on the right-hand side of Eq. (2) accounts for the modulation rate of the optical-klystron spectrum [28], while the second one reproduces the temporal profile of the electron bunch distribution. The latter is therefore assumed to keep its "natural" Gaussian profile under the action of the laser onset. This hypothesis also entails that the interaction of the electron beam with the ring environment [29–31] is neglected. This point will be further discussed in the following.

Defining $g_{0,n}$ as the peak gain after the nth interaction $g_n(\tau)$ can be written in the form

$$g_n(\tau) = g_{0,n} \exp\left[- \frac{\tau^2}{2\sigma_{\tau,n}^2} \right]. \qquad (3)$$

The evolution of the laser-induced energy spread is ruled by the following equation:

$$\sigma_{n+1}^2 = \sigma_n^2 + \frac{2\Delta T}{\tau_s} (\gamma I_n + \sigma_0^2 - \sigma_n^2), \qquad (4)$$

where $\gamma = \sigma_e^2 - \sigma_0^2$. Here σ_e is the equilibrium value (i.e., that reached at the laser saturation) of the energy spread at the perfect tuning and ΔT is the bouncing period of the laser inside the optical cavity; $I_n = \int_{-\infty}^{\infty} y_n(\tau) d\tau$ is the laser intensity normalized to its equilibrium value (i.e., the saturation value for $\epsilon = 0$) and τ_s stands for the synchrotron damping time. Assuming that the saturation is achieved when the peak gain is equal to the cavity losses P, the following relation holds [32]:

$$P = g_i \frac{\sigma_0}{\sigma_e} \exp\left[- \frac{\sigma_e^2 - \sigma_0^2}{2\sigma_0^2} \right]. \qquad (5)$$

By inserting Eq. (5) into Eq. (3) a closed expression for the peak gain is obtained:

$$g_{0,n} = g_i \frac{\sigma_0}{\sigma_n} \left[\frac{P \sigma_e}{g_i \sigma_0} \right]^{(\sigma_n^2 - \sigma_0^2)/\gamma}. \qquad (6)$$

Relation (5) sets the equilibrium value of the beam energy spread as function of the quantities g_i and P, regarded as independent variables. An approximate closed expression for the ratio σ_e/σ_0 is also obtained by means of a perturbative analysis. Assume

$$\frac{\sigma_e}{\sigma_0} = 1 + h \qquad (7)$$

with h small. From Eq. (5) one gets

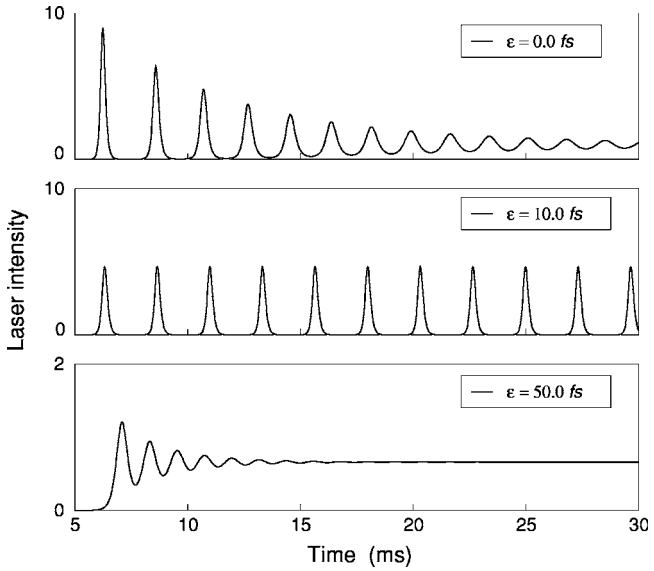

FIG. 4. Numerical simulation performed for the case of Super-ACO SRFEL. The results reproduce different "natural" regimes of the (normalized) laser intensity.

$$\ln\left(\frac{P}{g_i}\right) + h \simeq - \frac{1}{2}[(1+h)^2 - 1] \simeq - h \qquad (8)$$

and thus

$$\frac{\sigma_e}{\sigma_0} \simeq 1 + \frac{1}{2} \ln\left(\frac{g_i}{P}\right). \qquad (9)$$

This estimate is displayed in Fig. 3 and compared to a direct numerical solution of Eq. (5).

Finally, let us note that neglecting the interaction of the electron beam with the ring environment allows one to use, at any current, the relation of proportionality

$$\sigma_{\tau,n} = \frac{\alpha}{\Omega} \sigma_n, \qquad (10)$$

where Ω is the synchrotron frequency and α the momentum compaction factor.

The model presented in this section is shown to reproduce quantitatively the experimental results obtained on the Super-ACO FEL. This point was extensively addressed in Ref. [33]. As an example, in Fig. 4 the laser intensity is plotted as function of time: distinct dynamical regimes are found corresponding to different values of the detuning parameter ϵ.

III. THE EVOLUTION OF THE STATISTICAL PARAMETERS OF THE LASER DISTRIBUTION: AN EXPLICIT FORMULATION

Equation (1) governs the evolution of the statistical parameters of laser distribution, i.e., the laser intensity (zero-order moment), the laser centroid (first-order moment), and the standard deviation (second-order moment). By assuming a specific form of the laser distribution, it is in principle possible to characterize explicitly the dynamics of each

quantity. The choice of a Gaussian profile enables one to write

$$y_n(\tau) = \frac{I_n}{\sqrt{2\pi}\sigma_{l,n}} \exp\left[- \frac{(\tau - \tau_n)^2}{2\sigma_{l,n}^2} \right], \tag{11}$$

where I_n is the laser intensity, τ_n the position of the laser centroid, and $\sigma_{l,n}$ the r.m.s. width of the distribution. Note that the Gaussian hypothesis can be regarded as an extension of the result obtained in the framework of the super-mode theory [34] for a perfect laser-electron beam overlapping, to the case of a detuned FEL. Starting from this ansatz, the rate equations for the main statistical parameters are derived in the following. The details of the calculation are given in Ref. [35].

A. Laser intensity

The rate equation for the evolution of the laser intensity can be obtained by computing the zero-order moment of the laser distribution

$$\int_{-\infty}^{+\infty} y_{n+1}(\tau) d\tau = I_{n+1} = R^2 \int_{-\infty}^{+\infty} y_n(\tau - \epsilon)[1 + g_n(\tau)] d\tau + \int_{-\infty}^{+\infty} i_s(\tau) d\tau. \tag{12}$$

Making use of the assumption (11), one gets

$$I_{n+1} = R^2 I_n + R^2 \int_{-\infty}^{+\infty} y_n(\tau - \epsilon) g_n(\tau) d\tau + I_s, \tag{13}$$

where I_s is the intensity of the spontaneous emission normalized to the saturation value (at $\epsilon = 0$) of the laser intensity. By inserting Eq. (11) in Eq. (13), and computing the integral as in Ref. [36], one obtains the final equation

$$I_{n+1} = R^2 I_n \left\{ 1 + g_i \frac{\sigma_0}{\sigma_n} \frac{\exp\left[- \frac{\sigma_n^2 - \sigma_0^2}{2\sigma_0^2} \right] \exp\left[- \frac{(\tau_n + \epsilon)^2}{2(\sigma_{l,n}^2 + \sigma_{\tau,n}^2)} \right]}{\sqrt{1 + \left(\frac{\sigma_{l,n}}{\sigma_{\tau,n}} \right)^2}} \right\} + I_s. \tag{14}$$

B. Laser centroid

The rate equation for the evolution of the centroid of the laser distribution results from the calculation of its first-order moment

$$\begin{aligned} \int_{-\infty}^{+\infty} \tau y_{n+1}(\tau) d\tau &= I_{n+1} \tau_{n+1} \\ &= \frac{R^2 I_n}{\sqrt{2\pi}\sigma_{l,n}} \int_{-\infty}^{+\infty} \tau \times \exp\left[- \frac{(\tau - \tau_n - \epsilon)^2}{2\sigma_{l,n}^2} \right] d\tau + \frac{R^2 I_n}{\sqrt{2\pi}\sigma_{l,n}} g_i \frac{\sigma_0}{\sigma_n} \times \exp\left[- \frac{\sigma_n^2 - \sigma_0^2}{2\sigma_0^2} \right] \int_{-\infty}^{+\infty} \tau \\ &\quad \times \exp\left[- \frac{(\tau - \tau_n - \epsilon)^2}{2\sigma_{l,n}^2} \right] \times \exp\left[- \frac{\tau^2}{2\sigma_{\tau,n}^2} \right] d\tau + \int_{-\infty}^{+\infty} \tau i_s(\tau) d\tau. \end{aligned} \tag{15}$$

The last integral is equal to zero since the spontaneous emission is assumed to be a symmetric bell shaped function centered in $\tau = 0$. Further, it can be shown that

$$\frac{R^2 I_n}{\sqrt{2\pi}\sigma_{l,n}} \int_{-\infty}^{+\infty} \tau \exp\left[- \frac{(\tau - \tau_n - \epsilon)^2}{2\sigma_{l,n}^2} \right] d\tau = R^2 I_n (\tau_n + \epsilon) \tag{16}$$

and [36]

$$\begin{aligned} &\int_{-\infty}^{+\infty} \tau \exp\left[- \frac{(\tau - \tau_n - \epsilon)^2}{2\sigma_{l,n}^2} \right] \exp\left[- \frac{\tau^2}{2\sigma_{\tau,n}^2} \right] d\tau \\ &= \frac{\sqrt{2\pi}\sigma_{l,n}}{\sqrt{1 + \left(\frac{\sigma_{l,n}}{\sigma_{\tau,n}} \right)^2}} \frac{(\tau_n + \epsilon)}{1 + \left(\frac{\sigma_{l,n}}{\sigma_{\tau,n}} \right)^2} \exp\left[- \frac{(\tau_n + \epsilon)^2}{2(\sigma_{l,n}^2 + \sigma_{\tau,n}^2)} \right]. \end{aligned} \tag{17}$$

Combining together, one gets

$$\tau_{n+1} = (\tau_n + \epsilon) \frac{1 + J_0}{1 + J_0 \left[1 + \left(\frac{\sigma_{l,n}}{\sigma_{\tau,n}} \right)^2 \right]} \tag{18}$$

with

$$J_0 \equiv g_i \frac{\sigma_0}{\sigma_n} \frac{\exp\left[- \frac{\sigma_n^2 - \sigma_0^2}{2\sigma_0^2} \right] \exp\left[- \frac{(\tau_n + \epsilon)^2}{2(\sigma_{l,n}^2 + \sigma_{\tau,n}^2)} \right]}{\left[1 + \left(\frac{\sigma_{l,n}}{\sigma_{\tau,n}} \right)^2 \right]^{3/2}}. \tag{19}$$

Note that in deriving Eq. (18) we made explicit use of Eq. (14) and neglected the contribution associated to I_s.

C. Standard deviation

The evolution of the r.m.s. value of the laser distribution results from the calculation of its second-order moment

$$\begin{aligned} &\int_{-\infty}^{+\infty} (\tau - \tau_{n+1})^2 y_{n+1}(\tau) d\tau \\ &= I_{n+1} \sigma_{l,n+1}^2 \\ &= \frac{R^2 I_n}{\sqrt{2\pi}\sigma_{l,n}} \int_{-\infty}^{+\infty} (\tau - \tau_{n+1})^2 \times \exp\left[- \frac{(\tau - \tau_n - \epsilon)^2}{2\sigma_{l,n}^2} \right] d\tau + \frac{R^2 I_n}{\sqrt{2\pi}\sigma_{l,n}} g_i \frac{\sigma_0}{\sigma_n} \\ &\quad \times \exp\left[- \frac{\sigma_n^2 - \sigma_0^2}{2\sigma_0^2} \right] \int_{-\infty}^{+\infty} (\tau - \tau_{n+1})^2 \end{aligned}$$

$$\times \exp\left[-\frac{(\tau-\tau_n-\epsilon)^2}{2\sigma_{l,n}^2}\right]\exp\left[-\frac{\tau^2}{2\sigma_{\tau,n}^2}\right]d\tau + \int_{-\infty}^{+\infty}(\tau-\tau_{n+1})^2 i_s(\tau)d\tau. \quad (20)$$

Solving the integrals (see Ref. [35] for details) in the right-hand side of the previous equation, one gets

$$J_1 \equiv \frac{1}{\sqrt{2\pi}\sigma_{l,n}}\int_{-\infty}^{+\infty}(\tau-\tau_{n+1})^2\exp\left[-\frac{(\tau-\tau_n-\epsilon)^2}{2\sigma_{l,n}^2}\right]d\tau = \sigma_{l,n}^2+(\tau_n+\epsilon-\tau_{n+1})^2, \quad (21)$$

$$J_2 \equiv \frac{1}{\sqrt{2\pi}\sigma_{l,n}} g_i \frac{\sigma_0}{\sigma_n}\exp\left[-\frac{\sigma_n^2-\sigma_0^2}{2\sigma_0^2}\right]\int_{-\infty}^{+\infty}(\tau-\tau_{n+1})^2 \times\exp\left[-\frac{(\tau-\tau_n-\epsilon)^2}{2\sigma_{l,n}^2}\right]\exp\left[-\frac{\tau^2}{2\sigma_{\tau,n}^2}\right]d\tau$$
$$= g_i\frac{\sigma_0}{\sigma_n}\exp\left[-\frac{\sigma_n^2-\sigma_0^2}{2\sigma_0^2}\right]\frac{\exp\left[-\frac{(\tau_n+\epsilon)^2}{2(\sigma_{l,n}^2+\sigma_{\tau,n}^2)}\right]}{\left[1+\left(\frac{\sigma_{l,n}}{\sigma_{\tau,n}}\right)^2\right]^{1/2}} \times\left\{\frac{\sigma_{l,n}^2}{1+\left(\frac{\sigma_{l,n}}{\sigma_{\tau,n}}\right)^2}+\left[\frac{(\tau_n+\epsilon)}{1+\left(\frac{\sigma_{l,n}}{\sigma_{\tau,n}}\right)^2}-\tau_{n+1}\right]^2\right\}, \quad (22)$$

$$J_3 \equiv \int_{-\infty}^{+\infty}(\tau-\tau_{n+1})^2 i_s(\tau)d\tau = I_s(\sigma_{\tau,n}^2+\tau_{n+1}^2), \quad (23)$$

and Eq. (20) can be rewritten in the final compact form

$$\sigma_{l,n+1}^2 = \frac{R^2 I_n(J_1+J_2)+J_3}{I_{n+1}}. \quad (24)$$

Summing up, Eq. (1) is replaced by Eqs. (14), (18), and (24). The model needs still to be completed by Eq. (4), which governs the evolution of the laser-induced energy spread.

An exhaustive campaign of simulations has been performed in order to asses the validity of this new formulation. Systematic comparisons have been drawn with the original model using the case of the Super-ACO FEL as a reference (see Table I). A satisfactory agreement has been found [35], hence validating a posteriori the Gaussian hypothesis utilized in deriving Eqs. (14), (18), and (24).

Making the dynamics of the FEL parameters explicit offers some important advantages. First of all, a faster numerical implementation is now possible, thus enhancing the statistics over previous investigations. Moreover, and this is the main topic addressed in this paper, the new formulation opens up the perspective of a full analytical study, which allows us to characterize the functional dependence of the electron-beam energy spread, intensity, centroid position, and r.m.s. value of the laser distribution versus the light-electron beam detuning. In particular, it will be possible, through a stability analysis, to determine the critical value of the detuning parameter ϵ_c corresponding to the transition between the stable and unstable regimes. A concise survey of part of these results has been presented in Ref. [25].

TABLE I. Characteristics of the Super-ACO and ELETTRA SR-FELsfor a given experimental setting. The analytical dependence of I_s versus g_i and P (together with the numerical estimate reported here) has been obtained as in Ref. [35].

	Super ACO	Elettra
Beam energy (MeV)	800	900
α	1.4×10^{-2}	1.4×10^{-3}
Ω (KHz)	14	16
τ_s (ms)	8.5	87
σ_0	5.4×10^{-4}	1.5×10^{-5}
σ_e/σ_0	$\simeq$1.5	$\simeq$1.5
λ_{las} (nm)	350	250
g_i(%)	2	15
P(%)	0.8	7
ΔT (ns)	120	864
I_s	$\simeq1.4\times10^{-8}$	$\simeq4.3\times10^{-7}$

IV. A SIMPLIFIED FORMULATION

The previous formulation can be further simplified by restricting the analysis to relatively small values of the detuning ϵ. We are in particular interested in the region of stable ("cw") signal and we aim to characterize the transition to the unstable zone. Within this range, the quantities

$$x = \left(\frac{\sigma_{l,n}}{\sigma_{\tau,n}}\right)^2, \quad (25)$$

$$y = \frac{1}{2}\left(\frac{\tau_n+\epsilon}{\sigma_{\tau,n}}\right)^2 \quad (26)$$

are asymptotically small. These assumptions are supported by a numerical study based on the original model [33] and are also confirmed by experiments. Hence, a Taylor development can be performed in Eqs. (14), (18), and (24) derived above. In the following the analysis will be limited to the first order in both x and y. Mixed terms are also neglected.

A. Laser intensity

With $g_{0,n}$ defined as in Eq. (6), the rate equation for the laser intensity takes the form

$$I_{n+1} = R^2 I_n\left\{1+\frac{g_{0,n}\exp\left[\frac{-y}{1+x}\right]}{(1+x)^{1/2}}\right\}+I_s, \quad (27)$$

thus

$$I_{n+1} \simeq R^2 I_n\left[1+g_{0,n}\left(1-\frac{1}{2}x-y\right)\right]+I_s. \quad (28)$$

B. Laser centroid

Equation (18) can be written in the form

$$\tau_{n+1} = (\tau_n + \epsilon)\left[\frac{1 + g_{0,n}\dfrac{exp\left[\dfrac{-y}{1+x}\right]}{(1+x)^{3/2}}}{1 + g_{0,n}\dfrac{\exp\left[\dfrac{-y}{1+x}\right]}{(1+x)^{1/2}}}\right]. \tag{29}$$

Developing up to the first order in x and y, one gets

$$\tau_{n+1} = (\tau_n + \epsilon)[1 - g_{0,n}x], \tag{30}$$

where use has been made of the fact that $g_{0,n} \ll 1$.

C. Standard deviation

Equation (24) becomes

$$\sigma_{l,n+1}^2 = \frac{\sigma_{l,n}^2 + [(\tau_n + \epsilon) - \tau_{n+1}]^2 + \dfrac{g_{0,n}\exp\left[\dfrac{-y}{1+x}\right]}{(1+x)^{1/2}}\left[\dfrac{\sigma_{l,n}^2}{1+x} + \left(\dfrac{\tau_n + \epsilon}{1+x} - \tau_{n+1}\right)^2\right]}{1 + \dfrac{g_{0,n}\exp\left[\dfrac{-y}{1+x}\right]}{(1+x)^{1/2}}} + \frac{I_s(\sigma_{\tau,n}^2 + \tau_{n+1}^2)}{I_{n+1}}. \tag{31}$$

Developing up to the first order in x and y gives

$$\sigma_{l,n+1}^2 = \sigma_{l,n}^2[1 - g_{0,n}x] + \frac{I_s(\sigma_{\tau,n}^2 + \tau_n^2)}{I_n}, \tag{32}$$

where we operated the following additional simplification:

$$\frac{I_s}{I_{n+1}}(\sigma_{\tau,n}^2 + \tau_{n+1}^2) \simeq \frac{I_s}{I_n}(\sigma_{\tau,n}^2 + \tau_n^2). \tag{33}$$

D. The simplified 4D map

On the basis of the above, and recalling the definition of x and y introduced, respectively, in Eqs. (25) and (26), the simplified model accounting for the coupled evolution of the statistical longitudinal parameters of a SRFEL can be cast in the final form

$$\sigma_{n+1}^2 = \sigma_n^2 + \alpha_1[\alpha_2 I_n + 1 - \sigma_n^2],$$

$$I_{n+1} = R^2 I_n\left[1 + g_{0,n}\left(1 - \frac{\alpha_3}{2}\frac{\sigma_{l,n}^2}{\sigma_n^2} - \frac{\alpha_3}{2}\frac{(\tau_n + \epsilon)^2}{\sigma_n^2}\right)\right] + I_s,$$

$$\tau_{n+1} = (\tau_n + \epsilon)\left[1 - g_{0,n}\alpha_3\frac{\sigma_{l,n}^2}{\sigma_n^2}\right],$$

$$\sigma_{l,n+1}^2 = \sigma_{l,n}^2\left[1 - g_{0,n}\alpha_3\frac{\sigma_{l,n}^2}{\sigma_n^2}\right] + \frac{I_s}{I_n}\left(\frac{\sigma_n^2}{\alpha_3} + \tau_n^2\right), \tag{34}$$

where

$$\alpha_1 = \frac{2\Delta T}{\tau_s}, \quad \alpha_2 = \frac{\sigma_e^2 - \sigma_0^2}{\sigma_0^2}, \quad \alpha_3 = \left(\frac{\Omega}{\sigma_0 \alpha}\right)^2, \quad \alpha_4 = \frac{P\sigma_e}{g_i\sigma_0} \tag{35}$$

and

$$g_{0,n} = \frac{g_i}{\sigma_n}\left[\frac{P\sigma_e}{g_i\sigma_0}\right]^{(\sigma_n^2 - 1)/\alpha_2} = \frac{g_i}{\sigma_n}\alpha_4^{(\sigma_n^2 - 1)/\alpha_2}. \tag{36}$$

Note the redefinition of σ_n which is from hereon normalized to σ_0.

Although approximated, the model (34) still captures the main features of the longitudinal FEL dynamics. In particular, the transition from the "cw" regime to the unstable (pulsed) steady state occurs for a temporal detuning which is close to the one found in the framework of the exact formulation and, hence, to the experimental value. However, due to the approximations involved in the derivation, system (34) breaks down for large values of the detuning amount, i.e., when the lateral "cw" zones of the detuning curve are approached (see Fig. 4).

Consider now the phase space portraits $[z_n, (z_{n+1} - z_n)/\Delta T]$, where z stands for I, σ, τ, or σ_l. For small values of ϵ (i.e., when the laser spans the central "cw" zone of the detuning curve) the system tends asymptotically towards a stable fixed point, see Fig. 5. Beyond the transition to the unstable steady state, limit cycles are clearly displayed, see Fig. 6. This observation suggests the existence of a bifurcation occurring for a critical value ϵ_c of the detuning parameter. This issue will be extensively addressed in the following sections.

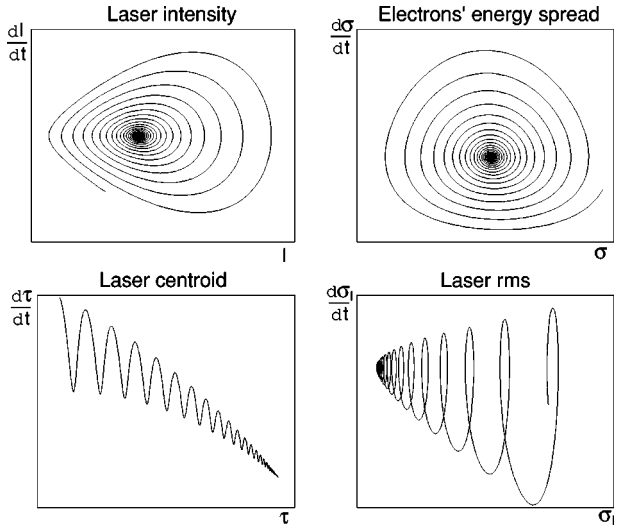

FIG. 5. Phase-space portraits for $\epsilon=0.1$ fs. Top left panel: $(I_{n+1}-I_n)/\Delta T$ versus I_n. Top right panel: $(\sigma_{n+1}-\sigma_n)/\Delta T$ versus σ_n. Bottom left panel: $(\tau_{n+1}-\tau_n)/\Delta T$ versus τ_n. Bottom right panel: $(\sigma_{l,n+1}-\sigma_{l,n})/\Delta T$ versus $\sigma_{l,n}$.

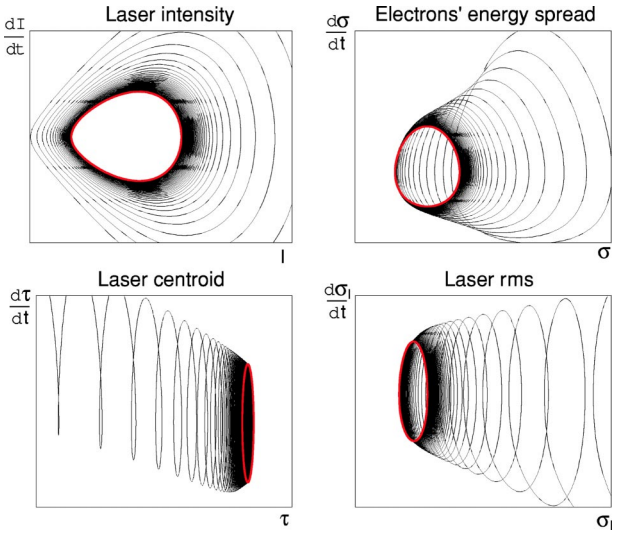

FIG. 6. Phase-space portraits for $\epsilon=2$ fs. Top left panel: $(I_{n+1}-I_n)/\Delta T$ versus I_n. Top right panel: $(\sigma_{n+1}-\sigma_n)/\Delta T$ versus σ_n. Bottom left panel: $(\tau_{n+1}-\tau_n)/\Delta T$ versus τ_n. Bottom right panel: $(\sigma_{l,n+1}-\sigma_{l,n})/\Delta T$ versus $\sigma_{l,n}$.

V. CALCULATION OF THE FIXED POINTS

By approximating finite differences with differentials, i.e.,

$$\frac{dI}{dt}\simeq\frac{I_{n+1}-I_n}{\Delta T},\quad \frac{d\sigma}{dt}\simeq\frac{\sigma_{n+1}-\sigma_n}{\Delta T},\quad \frac{d\tau}{dt}\simeq\frac{\tau_{n+1}-\tau_n}{\Delta T},\quad \frac{d\sigma_l}{dt}\simeq\frac{\sigma_{l,n+1}-\sigma_{l,n}}{\Delta T},\tag{37}$$

one can replace the single-turn map (34) with the continuous system

$$\frac{d\sigma}{dt}=\frac{\alpha_1}{\Delta T}\frac{1}{2\sigma}[\alpha_2 I+1-\sigma^2]\equiv f_1(\sigma,I,\tau,\sigma_l),$$

$$\frac{dI}{dt}=\frac{R^2}{\Delta T}I\left[-\frac{P}{R^2}+\frac{g_i}{\sigma}\alpha_4^{(\sigma^2-1)/\alpha_2}\left(1-\frac{\alpha_3}{2}\frac{\sigma_l^2}{\sigma^2}-\frac{\alpha_3}{2}\frac{(\tau+\epsilon)^2}{\sigma^2}\right)\right]+\frac{I_s}{\Delta T}\equiv f_2(\sigma,I,\tau,\sigma_l),$$

$$\frac{d\tau}{dt}=-\frac{\tau}{\Delta T}+\frac{(\tau+\epsilon)}{\Delta T}\left[1-g_i\alpha_3\alpha_4^{(\sigma^2-1)/\alpha_2}\frac{\sigma_l^2}{\sigma^3}\right]\equiv f_3(\sigma,I,\tau,\sigma_l),$$

$$\frac{d\sigma_l}{dt}=-\frac{1}{\Delta T}\frac{g_i}{2}\alpha_3\alpha_4^{(\sigma^2-1)/\alpha_2}\frac{\sigma_l^3}{\sigma^3}+\frac{1}{\Delta T}\frac{I_s}{I}\frac{1}{2\sigma_l}\left(\frac{\sigma^2}{\alpha_3}+\tau^2\right)\equiv f_4(\sigma,I,\tau,\sigma_l).\tag{38}$$

Assume from hereon $\epsilon>0$, being the scenario for $\epsilon<0$ completely equivalent. The fixed points $(\bar{I},\bar{\sigma},\bar{\tau},\bar{\sigma_l})$ of system (38) are found by imposing

$$\frac{dI}{dt}=\frac{d\sigma}{dt}=\frac{d\tau}{dt}=\frac{d\sigma_l}{dt}=0.\tag{39}$$

After some algebraic calculations, detailed in Appendix A, one can express $\bar{I},\bar{\tau},\bar{\sigma_l}$ as a function of $\bar{\sigma}$:

$$\bar{I}=\frac{\bar{\sigma}^2-1}{\alpha_2},\tag{40}$$

$$\bar{\tau}=\left\{\frac{1}{2}\left[-\frac{\bar{\sigma}^2}{\alpha_3}+\sqrt{\left(\frac{\bar{\sigma}^2}{\alpha_3}\right)^2+4\epsilon^2 A}\right]\right\}^{1/2},\tag{41}$$

$$\bar{\sigma_l}=\left\{\frac{I_s}{2g_i\alpha_3}\alpha_4^{(1-\bar{\sigma}^2)/\alpha_2}\alpha_2\frac{\bar{\sigma}^3}{\bar{\sigma}^2-1}\left[\frac{\bar{\sigma}^2}{\alpha_3}+\sqrt{\left(\frac{\bar{\sigma}^2}{\alpha_3}\right)^2+4\epsilon^2 A}\right]\right\}^{1/4},\tag{42}$$

where

$$A=\frac{\bar{\sigma}^3(\bar{\sigma}^2-1)}{\alpha_2 I_s}\frac{\alpha_4^{(1-\bar{\sigma}^2)/\alpha_2}}{g_i\alpha_3}.\tag{43}$$

The equilibrium value of the energy spread $\bar{\sigma}$ is found by solving the following implicit equation:

$$\frac{g_i}{\bar{\sigma}}\alpha_4^{(\bar{\sigma}^2-1)/\alpha_2}\left\{1-\frac{1}{2}\frac{\alpha_3}{\bar{\sigma}^2}[\bar{\sigma}_2^2+(\bar{\tau}+\epsilon)^2]\right\}=\frac{P}{R^2},\tag{44}$$

where $\bar{\sigma_l}$ and $\bar{\tau}$ are, respectively, given by Eqs. (42) and (41). Equation (44) can be solved numerically, for any given value of the detuning ϵ. The estimate of $\bar{\sigma}$ is then inserted in Eqs. (40)–(42), to compute the corresponding values of $\bar{I},\bar{\tau},\bar{\sigma_l}$. In Fig. 7 the asymptotic values of the main statistical parameters are plotted as a function of ϵ. The symbols refer to the simulations, while the solid line represents the above analytic solution. The agreement is remarkably good.

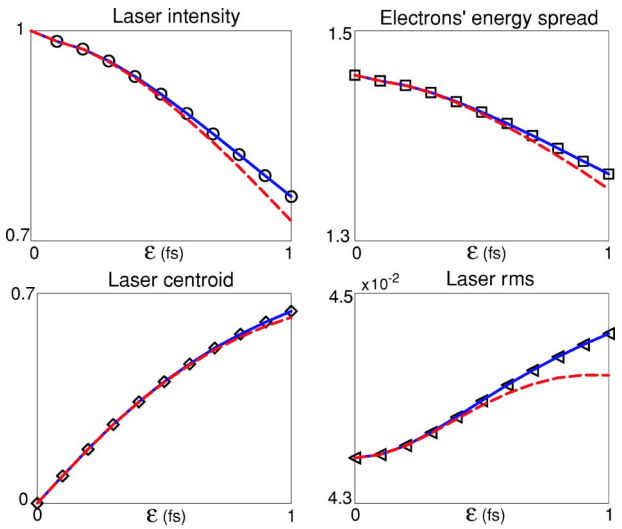

FIG. 7. The fixed points are plotted as function of the detuning parameter ϵ. Top left panel: Normalized laser intensity. Top right panel: Normalized electron-beam energy spread. Bottom left panel: Laser centroid. Bottom right panel: r.m.s. value of the laser distribution. The symbols refer to the simulations, the solid line stands for the analytic approach based on the numerical solution of Eq. (44), while the long-dashed lines represent the closed analytical expressions.

Furthermore, it is possible to derive a closed analytical expression for $\overline{\sigma}$ as a function of ϵ, and consequently for the whole bunch of variables involved, given the explicit relations (40)–(42). The details of the quite cumbersome calculation are enclosed in Appendix A. Here, attention is focused on the final result. Assume that the equilibrium value of the energy spread for $\epsilon \neq 0$ remains close to that reached at the perfect tuning

$$\overline{\sigma^2} = \frac{\sigma_e^2}{\sigma_0^2} + \delta \tag{45}$$

with $\delta \ll 1$. By inserting this ansatz in Eq. (44) and solving the system one gets

$$\delta = \frac{\dfrac{\sigma_e P}{\alpha_4 g_i \sigma_0 R^2} - 1 + \dfrac{1}{2}\alpha_3 \dfrac{\sigma_0^2}{\sigma_e^2}\Gamma_1}{\left(\dfrac{\ln \alpha_4}{\alpha_2} - \dfrac{1}{2}\dfrac{\sigma_0^2}{\sigma_e^2}\right)\left(1 - \dfrac{1}{2}\alpha_3 \dfrac{\sigma_0^2}{\sigma_e^2}\Gamma_1\right) - \dfrac{1}{2}\alpha_3 \dfrac{\sigma_0^2}{\sigma_e^2}\left(\Gamma_2 - \dfrac{\sigma_0^2}{\sigma_e^2}\Gamma_1\right)} \tag{46}$$

with

$$\Gamma_1 = \frac{1}{2}\left(-\frac{1}{\alpha_3}\frac{\sigma_e^2}{\sigma_0^2} + \sqrt{c}\right), \tag{47}$$

$$\Gamma_2 = \frac{1}{2}\left(-\frac{1}{\alpha_3} + \frac{1}{2}\frac{\dfrac{2}{\alpha_3^2}\dfrac{\sigma_e^2}{\sigma_0^2} + 4\epsilon^2 b}{\sqrt{c}}\right), \tag{48}$$

and

$$b = \frac{\sigma_e/\sigma_0}{g_i I_s \alpha_2 \alpha_3 \alpha_4}\left[\frac{3}{2}\left(\frac{\sigma_e^2}{\sigma_0^2} - 1\right) + \frac{\sigma_e^2}{\sigma_0^2} - \frac{\ln \alpha_4}{\alpha_2}\frac{\sigma_e^2}{\sigma_0^2}\left(\frac{\sigma_e^2}{\sigma_0^2} - 1\right)\right], \tag{49}$$

$$c = \frac{1}{\alpha_3^2}\frac{\sigma_e^2}{\sigma_0^2} + 4a\epsilon^2, \tag{50}$$

$$a = \frac{\sigma_e/\sigma_0}{g_i I_s \alpha_2 \alpha_3 \alpha_4}\left[\left(\frac{\sigma_e^2}{\sigma_0^2} - 1\right)\frac{\sigma_e^2}{\sigma_0^2}\right]. \tag{51}$$

This solution is plotted in Fig. 7 with a long-dashed line, displaying satisfactory agreement with the results of the simulations. To our knowledge this study represents the very first attempt to characterize the analytic dependence of the equilibrium statistical parameters of the SRFEL versus the temporal detuning ϵ, over the whole central region of "cw" behavior. In the next section attention is focused on the case of perfect tuning (i.e., $\epsilon = 0$) and comparisons are drawn between the theoretical results derived above and analogous predictions obtained in the framework of the super-mode theory. Comparison with experiments are also outlined.

VI. THE CASE OF PERFECT TUNING: COMPARISON WITH EXPERIMENTS AND WITH THE THEORY OF SUPERMODES

When the light and the electron beam are perfectly synchronized at each pass inside the interaction region (i.e., $\epsilon = 0$), Eq. (42) reduces to Ref. [37]:

$$\overline{\sigma_l} = \left[\frac{I_s}{P}\frac{1}{\alpha_3^2}\overline{\sigma}^4\right]^{1/4}, \tag{52}$$

where use has been made of the second and fourth of relations (35). Using Eqs. (9) and (10) and the third of relations (35), the expression for σ_l takes the form

$$\overline{\sigma_l} \simeq \left(\frac{I_s}{P}\right)^{1/4}\left[1 + \frac{1}{2}\ln\left(\frac{g_i}{P}\right)\right]\sigma_{\tau,0}. \tag{53}$$

The expression (53) for $\overline{\sigma_l}$ can be compared both with experimental results and with the estimate $(\overline{\sigma_l})_{\mathrm{sm}}$ obtained within the framework of the super-mode theory [34]:

$$(\overline{\sigma_l})_{\mathrm{sm}} = \frac{1}{c}\frac{1}{2}\left(1 + 7 \times 10^{-3}\frac{N_d}{N}\right)\sqrt{\Delta_{ok}\sigma_{\tau,0}}, \tag{54}$$

where $\Delta_{ok} = 2\Delta[1 + 0.913(N_d/N)]$, $\Delta = N\lambda_{\mathrm{las}}$ and λ_{las} stands for the laser wavelength.

In Table II the theoretical predictions $\overline{\sigma_l}$ and $(\overline{\sigma_l})_{\mathrm{sm}}$ are listed together with the experimental values obtained, for the settings of Table I, in the case of the Super-ACO and ELETTRA FELs.

The theoretical estimates based on Eq. (53) show to be closer by a factor 2 to the experimental values with respect to the results obtained in the framework of the super-mode theory. In addition, it is worth stressing that while relation (54) has been obtained in Ref. [34] by means of a semianalytical approach, relation (53) is fully analytical and allows

TABLE II. Theoretical widths of the laser pulse [obtained using relations (53) and (54)] compared to experimental values for the case of the Super-ACO and ELETTRA FELs. The experimental settings are those specified in Table I.

	Super ACO	Elettra
$\overline{\sigma_l}$ (ps)	5	2
$(\overline{\sigma_l})_{\mathrm{sm}}$ (ps)	2.5	1
Experimental values (ps)	$\simeq 9$	$\simeq 5$

us to relate the pulse width to the values of the independent variables of the model.

The results reported in Table II also indicate that the theoretical predictions underestimate in both cases the experimental value. The reason for that can be traced back to the fact that both theoretical models neglect the effect of the microwave instability resulting from the electron beam interaction with the ring environment (e.g., the metallic wall of the vacuum chamber) [29]. In the case of ELETTRA the situation is even more complicated by the presence of a "kick-like" instability (having a characteristic frequency of 50 Hz) which periodically switches off the laser preventing the attainment of a stable "cw" regime. A rigorous, self-consistent, analytical treatment of the SRFEL dynamics in presence of electron-beam instabilities is still lacking and will be addressed in a forthcoming analysis.

VII. STABILITY OF THE FIXED POINTS

The stability of the fixed point $\overline{\mathbf{X}} = [\overline{I}(\epsilon), \overline{\sigma}(\epsilon), \overline{\tau}(\epsilon), \overline{\sigma_l}(\epsilon)]$ can be determined by studying the eigenvalues of the Jacobian matrix associated to the system (38), namely,

$$\mathbf{J} = \begin{pmatrix} J_{11} & J_{12} & J_{13} & J_{14} \\ J_{21} & J_{22} & J_{23} & J_{24} \\ J_{31} & J_{32} & J_{33} & J_{34} \\ J_{41} & J_{42} & J_{43} & J_{44} \end{pmatrix}, \tag{55}$$

where

$$J_{ij} = \left(\frac{\partial f_i}{\partial X_j} \right)_{\mathbf{X}=\overline{\mathbf{X}}} \quad (i,j = 1,2,3,4), \tag{56}$$

where $\mathbf{X} = [\sigma, I, \tau, \sigma_l]$. The explicit expressions for the elements J_{ij} are given in Appendix B. The eigenvalues of the Jacobian are found by solving the fourth-order characteristic equations

$$\lambda^4 + c_3\lambda^3 + c_2\lambda^2 + c_1\lambda + c_0 = 0 \tag{57}$$

with

$$c_3 = -J_{11} - J_{22} - 3J_{33},$$

$$c_2 = 3J_{22}J_{33} - J_{21}J_{12} + J_{11}J_{22} + 2J_{33}^2 + 3J_{11}J_{33} - J_{42}J_{24} - J_{34}J_{43} \simeq -J_{21}J_{12}, \tag{58}$$

$$c_1 = J_{42}J_{24}J_{33} - 3J_{11}J_{22}J_{33} + 3J_{21}J_{12}J_{33} - J_{42}J_{23}J_{34} - 2J_{11}J_{33}^2 - J_{31}J_{12}J_{23} - 2J_{22}J_{33}^2 + J_{11}J_{42}J_{24} - J_{41}J_{12}J_{24} + J_{22}J_{34}J_{43} + J_{11}J_{34}J_{43} \simeq 3J_{21}J_{12}J_{33},$$

$$c_0 = -J_{11}J_{42}J_{24}J_{33} - J_{41}J_{12}J_{23}J_{34} - 2J_{21}J_{12}J_{33}^2 + 2J_{31}J_{12}J_{23}J_{33} + 2J_{11}J_{22}J_{33}^2 + J_{41}J_{12}J_{24}J_{33} + J_{11}J_{42}J_{23}J_{34} - J_{11}J_{22}J_{34}J_{43} + J_{21}J_{12}J_{34}J_{43} - J_{31}J_{12}J_{24}J_{43} \simeq -2J_{21}J_{12}J_{33}^2. \tag{59}$$

Equation (57) is solved numerically. The real and imaginary parts of the eigenvalues are reported in Fig. 8. The system is by definition stable when all the real parts of the eigenvalues are negative. The transition to an unstable regime occurs when at least one out of those becomes positive. In general, the loss of stability takes place according to different modalities. Consider, for instance, a Jacobian matrix with a pair of complex conjugate eigenvalues and assume the real parts of all the eigenvalues to be negative. A Hopf bifurcation occurs when the real part of the two complex eigenvalues become positive, provided the other keep their sign unchanged [38]. This situation is clearly displayed in Fig. 8, thus allowing us to conclude that the transition between the "cw" and the pulsed regime in a SRFEL is a Hopf bifurcation. These results allow the possibility of stabilizing the laser signal in the region where it displays a natural pulsed regime. This issue will be shortly addressed in the next section (see also Ref. [25]).

Finally, note that, in principle, the analytical characterization of $\overline{\mathbf{X}}$ given in Sec. V, allows us to directly estimate the eigenvalues. Hence, it should be possible to derive an approximate relation for the critical detuning ϵ. This crucial point will be addressed in the following.

VIII. STABILIZATION OF THE UNSTABLE STEADY STATE

Having characterized the transition from the stable to the unstable steady state in term of Hopf bifurcation opens up interesting perspectives for the improvement of the system performance. The procedure consists in introducing a specific self-controlled (closed loop) feedback to suppress locally the Hopf bifurcation and enlarge the zone of stable signal. This technique has been applied successfully in the past to stabilize the chaotic behavior of a conventional laser [39–41]. In the context of SRFEL, the control is achieved by replacing the constant detuning ϵ with the time-dependent quantity

$$\epsilon(t) = \epsilon_0 + \beta \Delta T \dot{I} \tag{60}$$

(where $\dot{I}$ stands for the time derivative of the laser intensity), which is added to the system (38).

Here ϵ_0 is assumed to be larger than ϵ_c: when the control is switched off, i.e., $\beta = 0$, the laser is therefore unstable and displays periodic oscillations. For β larger than a certain threshold β_c, the oscillations are damped and the laser behaves as if it were in the "cw" region. Note that, as soon as the saturation is reached, $\dot{I} = 0$ and, thus, the stable regime is

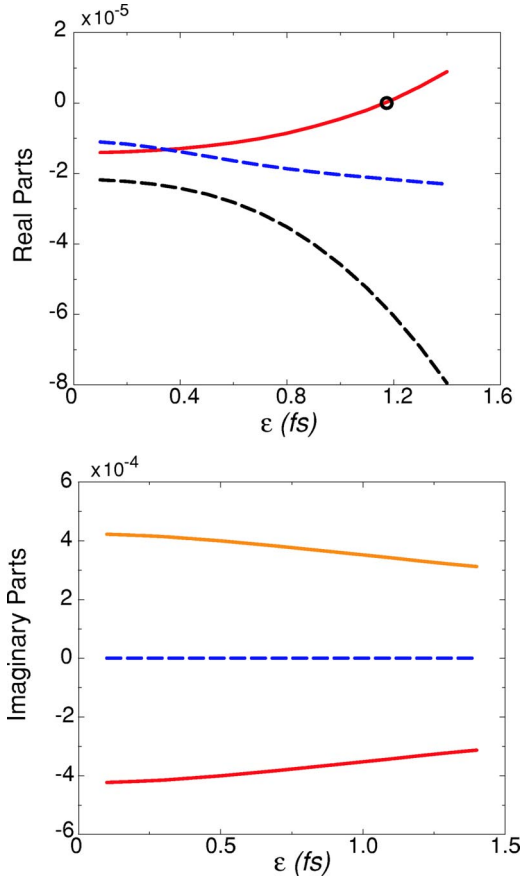

FIG. 8. Real (upper panel) and imaginary (lower panel) parts of the eigenvalues of the Jacobian matrix associated to the system (38) as a function of the detuning parameter ϵ. The circle in the picture for the real parts represents the transition from the stable to the pulsed regime, i.e., the Hopf bifurcation.

maintained asymptotically for $\epsilon=\epsilon_0>\epsilon_c$, i.e., well in the former unstable zone. Figure 9 shows the behavior of the FEL intensity obtained for, respectively, $\beta=0$ (control off) and $\beta=6\times10^{-3}$ (control on). Here $\beta_c\sim5\times10^{-4}$.

This theoretical result provides the ground for experimental tests, aiming to enlarge the stable "cw" zone of the detuning curve. An outline of the strategy is depicted below. The signal proportional to the total output power (produced, e.g., by the response of a photodiode) is sent to the stabilization system, made of a simple device to obtain a derivative, followed by an inverting amplifier with a variable gain. The output of the feedback system is then used to modify the electron-beam revolution period (via the modification of the radio frequency), i.e., the value of the detuning ϵ. Recently, this technique has been applied at Super-ACO [42] and ELETTRA [43] and shown to produce a significant extension of the stable "cw" region, thus confirming our theoretical predictions.

IX. CALCULATION OF THE CRITICAL DETUNING PARAMETER

The knowledge of the eigenvalues of the Jacobian matrix (56) as a function of ϵ allows us to derive the value of ϵ_c, for

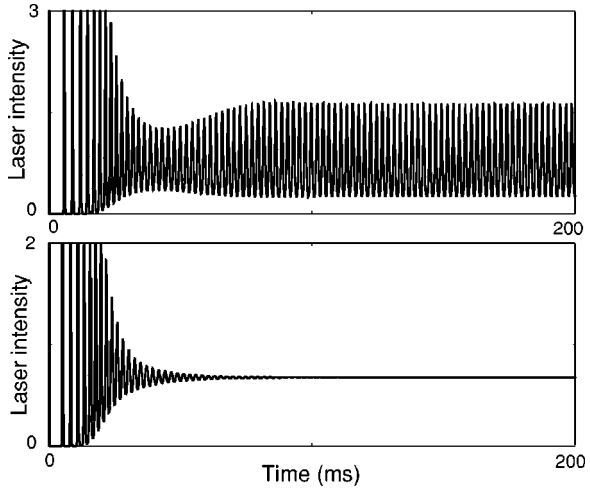

FIG. 9. Behavior of the FEL intensity in absence (upper panel) and in presence (lower panel) of the derivative control system. The parameters utilized for the simulations are those of Super-ACO (see Table I). The value of ϵ_0 [see Eq. (60)] has been set to 1.3 fs, i.e., well inside the unstable region of the detuning curve. The stabilization has been achieved using $\beta=6\times10^{-3}$.

any given experimental setting. In Fig. 10, ϵ_c is plotted versus the ratio g_i/P. The circles refers to the values determined from dynamical simulations, while the diamonds stand for the computation. The agreement is good.

Further, as previously mentioned, it is is principle possible to obtain an approximate relation for ϵ_c, by using the closed analytical expressions for the fixed points, derived in Sec. V. Assume Eq. (57) to admit two purely imaginary solutions, i.e., $\lambda=\pm i\omega$ (with $\omega\in\mathrm{Re}$). By definition, this condition holds when $\epsilon=\epsilon_c$. Equation (57) reduces to

$$\omega^4-c_2\omega^2+c_0=0,$$

$$-c_3\omega^3+c_1\omega=0. \tag{61}$$

By inserting the solution of the first of Eq. (61) into the second, and taking into account that numerical evidences suggest $c_0\ll c_2$, one gets

$$0=-\frac{1}{2}c_3(c_2+\sqrt{c_2^2-4c_0})+c_1\simeq-c_2c_3+\frac{c_0c_3}{c_2}+c_1$$

$$\simeq-J_{21}J_{12}(J_{11}+J_{22}+3J_{33})-\frac{(J_{11}+J_{22}+3J_{33})2J_{21}J_{12}J_{33}^2}{J_{21}J_{12}}$$

$$+3J_{21}J_{12}J_{33}=-(J_{11}+J_{22})(J_{21}J_{12}+2J_{33}^2)-6J_{33}^3. \tag{62}$$

By making use of the explicit expressions given in Appendix B, it can be shown that J_{33} is much smaller than J_{11}, J_{22}, J_{21}, and J_{12}, and thus the previous equation reduces to

$$(J_{11}+J_{22})\simeq0. \tag{63}$$

Recalling Eqs. (B2) and (B7) in Appendix B, the equation for ϵ_c takes the final form

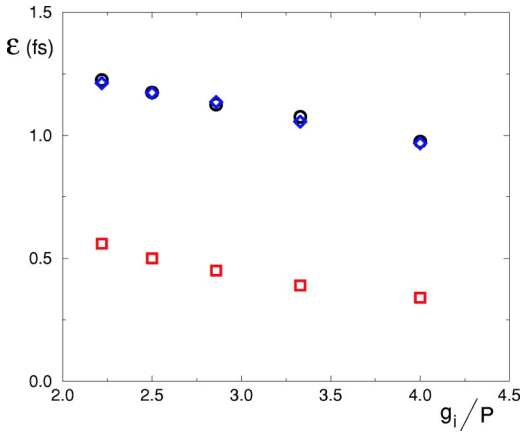

FIG. 10. ϵ_c is plotted versus the ratio g_i/P. The circles stand for the simulations. The diamonds represent the exact numerical study. The squares refer to the approximate analytical expression (66). Simulations refer to the case of Super-ACO.

$$-\alpha_1 + R^2\left\{1 + \frac{g_i}{\overline{\sigma}}\alpha_4^{(\overline{\sigma}-1)/\alpha_2}\left[1 - \frac{\alpha_3}{2}\left(\frac{\overline{\sigma_2^t}}{\overline{\sigma^2}} + \frac{(\overline{\tau}+\epsilon_c)^2}{\overline{\sigma^2}}\right)\right]\right\} - 1 \simeq 0. \tag{64}$$

For the purpose of evaluating ϵ_c, one can neglect the contribution of the correction δ in the expression (45) for $\overline{\sigma}$. Thus, according to Eq. (9), $\overline{\sigma} \simeq \sigma_e/\sigma_0 \simeq 1 + 1/2\ \ln(g_i/P)$.

Moreover, taking into account that $\overline{\sigma_2^t} \ll \overline{\tau^2}$ and that $\epsilon_c \ll \overline{\tau}$, and recalling Eq. (41), one gets

$$\left(-\alpha_1 - P + \frac{5}{4}\frac{R^2 g_i}{\overline{\sigma}}\alpha_4\right)\frac{\overline{\sigma}}{g_i R^2}\frac{4}{\alpha_4} \simeq \sqrt{1 + \frac{4\epsilon_c^2 A}{(\overline{\sigma^2}/\alpha_3)^2}}, \tag{65}$$

that is, making use of Eq. (43),

$$\epsilon_c \simeq \frac{1}{4}\frac{\alpha_2\alpha_4 I_s g_i}{\alpha_3}\frac{\overline{\sigma}}{\overline{\sigma^2} - 1}\left\{\left[5 - \frac{4\overline{\sigma}(P+\alpha_1)}{\alpha_4 R^2 g_i}\right]^2 - 1\right\}. \tag{66}$$

The values computed using relation (65) are plotted in Fig. 10 (squares), for different values of g_i/P. Even though a discrepancy is observed, Eq. (66) is able to reproduce the qualitative behavior of the simulated data. Hence, it represents a reliable tool to investigate the extension of the stable zone as function of the main parameters of the system. Note that the explicit knowledge of the critical detuning may allow to exploit the range of tunability of the machine parameters, thus obtaining the largest stable zone as a result of an optimization of the experimental setting.

In the framework of the super-mode theory a semianalytical expression for ϵ_c was recently derived [34], namely,

$$(\epsilon_c)_{\mathrm{sm}} = \frac{1.355}{c}\frac{\delta_l}{1 + \mu_c/\tilde{x}}, \tag{67}$$

where $\delta_l \simeq 0.114[1 + 0.015(N_d/N)]\Delta_{ok} g_i$ is the cavity mismatch yielding the maximum gain, $\mu_c = \Delta_{ok}/\sigma_{\tau,0}$ stands for the slippage factor and $\tilde{x} = 3 + 0.1(N_d/N)$.

The different theoretical estimates can be compared to the experimental results. The values are listed in Table III for the case of the Super-ACO FEL.

TABLE III. Theoretical values of the critical detuning value calculated using the set of parameters specified in Table I and compared, for the case of the Super-ACO FEL, with experimental results. Here $\epsilon_c^{\mathrm{exact}}$ refers to the exact calculation (diamonds in Fig. 10) while $\epsilon_c^{\mathrm{approx}}$ stands to the approximate analytical expression (66); $(\epsilon_c)_{\mathrm{sm}}$ has been calculated using Eq. (67).

	Super ACO
$\epsilon_c^{\mathrm{exact}}$(fs)	1
$\epsilon_c^{\mathrm{approx}}$(fs)	0.5
$(\epsilon_c)_{\mathrm{sm}}$(fs)	2
Experimental value (fs)	1–4

A comparison with experiments is possible only for the case of the Super-ACO FEL. As it has been already remarked, the ELETTRA FEL does not presently display a stable "cw" zone around the perfect synchronism. As shown in Table I, a satisfactory agreement between theory and experiments is found, even though relation (66) slightly underestimates the real value. However, it is again worth stressing that while Eq. (67) has been found by means of a semianalytical calculation, relation (66) is fully analytical and allows us to relate the critical detuning parameter to the values of the independent variables of the model.

X. CONCLUSIONS

The results obtained in this paper are manifold. Based on the assumption of Gaussianity of the laser profile, a new approximate model of SRFEL has been derived. This simplified formulation enables a deeper analytical insight into the longitudinal dynamics of a detuned SRFEL. This allows us, in particular, to characterize the saturated statistical parameters as a function of the detuning amount and to determine the critical detuning at the point of transition between stable and unstable regimes. Theoretical results have been compared to the estimates obtained in the framework of the super-mode theory and shown to be in good agreement with experiments.

Moreover, the transition between the stable "cw" regime and the unstable steady state has been shown to be a Hopf bifurcation. Hence, a suitable feedback procedure has been introduced and shown to enlarge the region of stable signal. This theoretical result opens up the perspective of improving the performance of the real device, in terms of stability and efficiency.

ACKNOWLEDGMENTS

We are particularly thankful to M. Billardon, who inspired this work, and to the Super-ACO FEL group headed by M. E. Couprie. Discussions with M. Basso, N. Berglund, G. Dattoli, B. Diviacco, L. Giannessi, R. Meucci, M. Pettini, and M. Trovò are acknowledged. D. F. thanks U. Skoglund for stimulating discussions and good advice. D.F. gratefully acknowledges M. Bianchini from Edison Giocattoli (Florence), for expressing his interest in this research. G. D. N. acknowl-

edges the support given by EUFELE, a project funded by the European Commission under FP5 Contract No. HPRI-CT-2001-50025.

APPENDIX A: CALCULATION OF THE FIXED POINTS OF SYSTEM (38)

Consider the system (34). The fixed points are found by solving the following set of equations:

$$\alpha_2 \overline{I} + 1 - \overline{\sigma^2} = 0,$$

$$R^2\left[1 + \frac{g_i}{\overline{\sigma}}\alpha_4^{(\overline{\sigma^2}-1)/\alpha_2}\left(1 - \frac{\alpha_3}{2}\frac{\overline{\sigma_l^2}}{\overline{\sigma^2}} - \frac{\alpha_3}{2}\frac{(\overline{\tau}+\epsilon)^2}{\overline{\sigma^2}}\right)\right] = 1,$$

$$(\overline{\tau}+\epsilon) g_i \alpha_3 \alpha_4^{(\overline{\sigma^2}-1)/\alpha_2}\frac{\overline{\sigma_l^2}}{\overline{\sigma^3}} = \epsilon,$$

$$g_i \alpha_3 \alpha_4^{(\overline{\sigma^2}-1)/\alpha_2}\frac{\overline{\sigma_l^4}}{\overline{\sigma^3}} = \frac{I_s}{\overline{I}}\left(\frac{\overline{\sigma^2}}{\alpha_3} + \overline{\tau^2}\right). \tag{A1}$$

By dividing, side by side, the third and the fourth equations of Eq. (A1), one gets

$$\frac{(\overline{\tau}+\epsilon)}{\overline{\sigma_l^2}} = \frac{\epsilon \overline{I}}{I_s}\frac{1}{\left(\frac{\overline{\sigma^2}}{\alpha_3} + \overline{\tau^2}\right)}. \tag{A2}$$

Neglecting ϵ with respect to $\overline{\tau}$, the previous equation can be written in the form

$$\overline{\tau^3} + \frac{\overline{\sigma^2}}{\alpha_3}\overline{\tau} = \frac{\epsilon \overline{\sigma_2^\dagger} \overline{I}}{I_s}. \tag{A3}$$

From the third equation of the system (A1), one gets

$$\overline{\sigma_2^\dagger} = \frac{\epsilon}{g_i \alpha_3}\frac{\overline{\sigma^3}}{(\overline{\tau}+\epsilon)}\alpha_4^{(1-\overline{\sigma^2})/\alpha_2} \simeq \frac{\epsilon}{g_i \alpha_3}\frac{\overline{\sigma^3}}{\overline{\tau}}\alpha_4^{(1-\overline{\sigma^2})/\alpha_2}. \tag{A4}$$

Substituting (A4) into (A3) gives

$$\overline{\tau^4} + \frac{\overline{\sigma^2}}{\alpha_3}\overline{\tau^2} = \frac{\epsilon^2 \overline{I}}{I_s}\frac{\overline{\sigma^3}\alpha_4^{(1-\overline{\sigma^2})/\alpha_2}}{g_i \alpha_3}. \tag{A5}$$

On the other hand, from the first equation of the system (A1), one obtains

$$\overline{I} = \frac{\overline{\sigma^2} - 1}{\alpha_2} \tag{A6}$$

[which coincides with Eq. (40)].

The fourth-order equation for $\overline{\tau}$ can be finally written in the form

$$\overline{\tau^4} + \frac{\overline{\sigma^2}}{\alpha_3}\overline{\tau^2} = A\epsilon^2, \tag{A7}$$

where the coefficient A is defined as in Eq. (43). Solving Eq. (A7), one gets the result (41).

Consider now the fourth equation of the system (A1). Using the expression (41) for $\overline{\tau}$, one finds Eq. (42) for $\overline{\sigma_l}$.

An approximated closed analytical expression for $\overline{\sigma}$ can be also derived by assuming

$$\overline{\sigma^2} = \frac{\sigma_e^2}{\sigma_0^2} + \delta \tag{A8}$$

(with $\delta \ll 1$) and solving Eq. (44) for δ. The main steps of the calculation are outlined below.

First, the following approximations hold:

$$\overline{\sigma} = \sqrt{\frac{\sigma_e^2}{\sigma_0^2}\left(1 + \frac{\delta}{\sigma_e^2/\sigma_0^2}\right)} \simeq \frac{\sigma_e}{\sigma_0}\left(1 + \frac{1}{2}\frac{\sigma_0^2}{\sigma_e^2}\delta\right), \tag{A9}$$

$$\alpha_4^{(\overline{\sigma^2}-1)/\alpha_2} \simeq \alpha_4 \alpha_4^{\delta/\alpha_2} \simeq \alpha_4\left(1 + \frac{\ln \alpha_4}{\alpha_2}\delta\right), \tag{A10}$$

$$\frac{1}{\overline{\sigma^2}} \simeq \frac{\sigma_0^2}{\sigma_e^2}\left(1 - \frac{\sigma_0^2}{\sigma_e^2}\delta\right). \tag{A11}$$

By making use of relations (A9)–(A11), one gets

$$A = \frac{\overline{\sigma^3}(\overline{\sigma^2}-1)}{\alpha_2 I_s}\frac{\alpha_4^{(1-\overline{\sigma^2})/\alpha_2}}{g_i \alpha_3} \simeq \frac{\sigma_e^2/\sigma_0^2}{g_i I_s \alpha_3 \alpha_4}\left[\left(\frac{\sigma_e^2}{\sigma_0^2} - 1\right) + \delta\right] \times \left(\frac{\sigma_e^2}{\sigma_0^2} + \delta\right)\left(1 + \frac{1}{2}\frac{\sigma_e^2}{\sigma_0^2}\delta\right)\left(1 - \frac{\ln \alpha_4}{\alpha_2}\delta\right)$$

which, at the first order in δ, takes the form

$$A \simeq a + \delta b \tag{A12}$$

with a and b given, respectively, by Eqs. (51) and (49).

Further, by inserting Eq. (A12) into (41) and retaining only the first order terms in δ one gets

$$\overline{\tau^2} = \Gamma_1 + \delta \Gamma_2, \tag{A13}$$

with Γ_1 and Γ_2 as in Eqs. (47) and (48).

Finally, the second equation of the system (A1) can be recast in the form

$$\frac{g_i}{\overline{\sigma}}\alpha_4^{(\overline{\sigma^2}-1)/\alpha_2}\left\{1 - \frac{1}{2}\frac{\alpha_3}{\overline{\sigma^2}}\left[\overline{\sigma_l^2} + (\overline{\tau}+\epsilon)^2\right]\right\} = \frac{P}{R^2}. \tag{A14}$$

By inserting both Eqs. (A12) and (A13) into Eq. (A14) and solving for δ one ends up with relation (46).

APPENDIX B: CALCULATION OF JACOBIAN MATRIX OF SYSTEM (38)

In this Appendix the elements

$$J_{ij} = \left(\frac{\partial f_i}{\partial X_j}\right)_{\mathbf{X}=\overline{\mathbf{X}}} \quad (i,j = 1,2,3,4) \tag{B1}$$

of the Jacobian matrix associated to the single-turn map (38), are listed. A straightforward calculation leads to

$$J_{11} = -\frac{\alpha_1}{\Delta T}, \tag{B2}$$

$$J_{12} = \frac{\alpha_1 \alpha_2}{\Delta T}, \tag{B3}$$

$$J_{13} = 0, \tag{B4}$$

$$J_{14} = 0; \tag{B5}$$

$$J_{21} = \frac{R^2}{\Delta T}\frac{g_i}{\bar{\sigma}}\bar{I}\alpha_4^{(\bar{\sigma}^2-1)/\alpha_2}\left\{\left[\frac{\ln\alpha_4}{\alpha_2} - \frac{1}{2\bar{\sigma}}\right] \times\left[1 - \frac{\alpha_3}{2}\left(\frac{\bar{\sigma}_2^2}{\bar{\sigma}^2} + \frac{(\bar{\tau}+\epsilon)^2}{\bar{\sigma}^2}\right)\right] + \frac{\alpha_3}{2}\left(\frac{\bar{\sigma}_2^2}{\bar{\sigma}^4} + \frac{(\bar{\tau}+\epsilon)^2}{\bar{\sigma}^4}\right)\right\}, \tag{B6}$$

$$J_{22} = \frac{R^2}{\Delta T}\left\{1 + \frac{g_i}{\bar{\sigma}}\alpha_4^{(\bar{\sigma}^2-1)/\alpha_2}\left[1 - \frac{\alpha_3}{2}\left(\frac{\bar{\sigma}_l^2}{\bar{\sigma}^2} + \frac{(\bar{\tau}+\epsilon)^2}{\bar{\sigma}^2}\right)\right]\right\} - \frac{1}{\Delta T}, \tag{B7}$$

$$J_{23} = -\frac{R^2}{\Delta T}\alpha_3\frac{g_i}{\bar{\sigma}}\bar{I}\alpha_4^{(\bar{\sigma}^2-1)/\alpha_2}\frac{(\bar{\tau}+\epsilon)}{\bar{\sigma}^2}, \tag{B8}$$

$$J_{24} = -\frac{1}{2}\frac{R^2}{\Delta T}\alpha_3\frac{g_i}{\bar{\sigma}}\bar{I}\alpha_4^{(\bar{\sigma}^2-1)/\alpha_2}\frac{1}{\bar{\sigma}^2}; \tag{B9}$$

$$J_{31} = \frac{1}{\Delta T}\alpha_3\frac{g_i}{\bar{\sigma}}\alpha_4^{(\bar{\sigma}^2-1)/\alpha_2}(\bar{\tau}+\epsilon)\frac{\bar{\sigma}_l^2}{\bar{\sigma}^2}\left(\frac{\ln\alpha_4}{\alpha_2} - \frac{3}{2}\frac{1}{\bar{\sigma}^2}\right), \tag{B10}$$

$$J_{32} = 0, \tag{B11}$$

$$J_{33} = -\frac{1}{\Delta T}\alpha_3\frac{g_i}{\bar{\sigma}}\alpha_4^{(\bar{\sigma}^2-1)/\alpha_2}\frac{\bar{\sigma}_l^2}{\bar{\sigma}^2}, \tag{B12}$$

$$J_{34} = -\frac{1}{\Delta T}\alpha_3\frac{g_i}{\bar{\sigma}}\alpha_4^{(\bar{\sigma}^2-1)/\alpha_2}(\bar{\tau}+\epsilon)\frac{1}{\bar{\sigma}^2}; \tag{B13}$$

$$J_{41} = -\frac{1}{\Delta T}\alpha_3\frac{g_i}{\bar{\sigma}}\alpha_4^{(\bar{\sigma}^2-1)/\alpha_2}\frac{\bar{\sigma}_l^4}{\bar{\sigma}^2}\left(\frac{\ln\alpha_4}{\alpha_2} - \frac{3}{2}\frac{1}{\bar{\sigma}^2}\right) + \frac{1}{\Delta T}\frac{I_s}{\alpha_3\vec{I}} \tag{B14}$$

$$J_{42} = -\frac{1}{\Delta T}\frac{I_s}{\bar{I}^2}\left[\frac{\bar{\sigma}^2}{\alpha_3} + (\bar{\tau}+\epsilon)^2\right], \tag{B15}$$

$$J_{43} = \frac{2}{\Delta T}\frac{I_s(\bar{\tau}+\epsilon)}{\bar{I}}, \tag{B16}$$

$$J_{44} = 2J_{33}. \tag{B17}$$

[1] D. A. G. Deacon *et al.*, Phys. Rev. Lett. **38**, 892 (1977).
[2] M. Billardon *et al.*, Phys. Rev. Lett. **51**, 1652 (1983).
[3] C. Pellegrini, Nucl. Instrum. Methods Phys. Res. A **475**, 1 (2001).
[4] L. H. Yu, Phys. Rev. A **44**, 5178 (1991).
[5] M. E. Couprie *et al.*, Rev. Sci. Instrum. **65**, 1485 (1994).
[6] M. Marsi *et al.*, Appl. Phys. Lett. **70**, 895 (1997).
[7] M. E. Couprie *et al.*, Nucl. Instrum. Methods Phys. Res. A **331**, 37 (1993).
[8] H. Hama *et al.*, Nucl. Instrum. Methods Phys. Res. A **375**, 32 (1996).
[9] M. E. Couprie *et al.*, Nucl. Instrum. Methods Phys. Res. A **475**, 229 (2001).
[10] G. De Ninno *et al.*, ELETTRA internal Note ST/SL-03/01, 2003 (unpublished).
[11] G. De Ninno *et al.*, Nucl. Instrum. Methods Phys. Res. A **507**, 274 (2003).
[12] M. E. Couprie *et al.*, Nucl. Instrum. Methods Phys. Res. A **358**, 374 (1995).
[13] S. Koda *et al.*, Nucl. Instrum. Methods Phys. Res. A **475**, 211 (2001).
[14] G. Dattoli *et al.*, Phys. Rev. A **37**, 4326 (1988).
[15] G. Dattoli *et al.*, Phys. Rev. A **37**, 4334 (1988).
[16] V. N. Litvinenko, Nucl. Instrum. Methods Phys. Res. A **475**, 240 (2001).
[17] G. De Ninno *et al.*, Phys. Rev. E **64**, 026502 (2001).
[18] V. N. Litvinenko *et al.*, Nucl. Instrum. Methods Phys. Res. A **358**, 369 (1995).
[19] G. De Ninno *et al.*, Phys. Rev. E **64**, 026502 (2001).
[20] R. Bartolini *et al.*, ENEA internal Note, 2002 (unpublished).
[21] M. Billardon *et al.*, Phys. Rev. Lett. **69**, 2368 (1992).
[22] G. Dattoli *et al.*, Nucl. Instrum. Methods Phys. Res. A **365**, 559 (1995).
[23] G. De Ninno, D. Fanelli, and M. E. Couprie, Nucl. Instrum. Methods Phys. Res. A **483**, 177 (2002).
[24] C. Thomas *et al.*, Nucl. Instrum. Methods Phys. Res. A **483**, 181 (2002).
[25] G. De Ninno and D. Fanelli, Phys. Rev. Lett. **92**, 094801(2004).
[26] N. A. Vinokurov *et al.*, Report No. INP77.59, Novossibirsk, 1977 (unpublished).
[27] The case of SRFELsimplemented on an optical kylstron is considered here [26]. An optical klystron consists of two undulators separated by a dispersive section (i.e., a strong magnetic field) favoring the interference between the emission of the two undulators.
[28] The laser-off peak gain has been optimized by assuming $N + N_d = 1/(4\pi\sigma_0)$ in the expression of the modulation rate, where N is the periods' number of the undulators of the optical klystron and N_d is the interference order due to its dispersive section.
[29] G. Dattoli and A. Renieri, Nucl. Instrum. Methods Phys. Res. A **375**, 1 (1996).
[30] M. Migliorati and L. Palumbo, Nuovo Cimento Soc. Ital. Fis., A **112**, 461 (1999).
[31] H. Hama *et al.*, Nucl. Instrum. Methods Phys. Res. A **341**, 12

(1994).
[32] As a function of the cavity losses, the mirror reflectivity R is given by $\sqrt{1-P}$.
[33] G. De Ninno *et al.*, Eur. Phys. J. D **22**, 269 (2003).
[34] G. Dattoli *et al.* (unpublished).
[35] G. De Ninno and D. Fanelli, Elettra Technical Report ST/SL-03/03, 2003 (unpublished).
[36] I. S. Gradshteyn and I. M. Ryzhik, *Table of Integrals, Series and Products* (Academic Press, London, 1980).
[37] It should be remarked that when $\epsilon=0$, then $\delta=1/R^2-1$. Thus, formally, $\overline{\sigma}(\epsilon=0)\neq\sigma_e/\sigma_0$, which is in apparent contradiction with the assumption of the model. However, since $R^2=1-P\sim 1$, thus $\delta(\epsilon=0)\sim 0$, the residual small discrepancy being related to the approximations involved in the calculation, see Appendix A.
[38] R. C. Hilborn, *Chaos and Nonlinear Dynamics* (Oxford University Press, Oxford, 1994).
[39] V. Petrov *et al.*, J. Chem. Phys. **96**, 7503 (1992).
[40] S. Bielawski *et al.*, Phys. Rev. E **49**, R971 (1994).
[41] M. Ciofini *et al.*, Phys. Rev. E **60**, 398 (1999).
[42] M. E. Couprie *et al.*, Nucl. Instrum. Methods Phys. Res. A (to be published).
[43] G. De Ninno *et al.* (in preparation).